Journal of Power Sources 195 (2010) 6510–6515

Contents lists available at ScienceDirect

Journal of Power Sources

journal homepage: www.elsevier.com/locate/jpowsour

Short communication

High sintering activity Cu–Gd co-doped CeO_2 electrolyte for solid oxide fuel cells

Yingchao Dong[a,*], Stuart Hampshire[a], Bin Lin[b], Yihan Ling[b], Xiaozhen Zhang[b]

[a] Materials and Surface Science Institute (MSSI), University of Limerick, Castletroy National Technological Park, Limerick, Ireland
[b] USTC Lab for Solid State Chemistry and Inorganic Membranes, Department of Materials Science and Engineering, University of Science and Technology of China (USTC), Hefei, 230026, PR China

ARTICLE INFO

Article history:
Received 26 December 2009
Received in revised form 22 February 2010
Accepted 14 March 2010
Available online 20 March 2010

Keywords:
Solid-oxide fuel cell
Ceria electrolyte
Sintering aid CuO
Combustion synthesis
Low-temperature sintering

ABSTRACT

Nano-sized $Ce_{0.79}Gd_{0.2}Cu_{0.01}O_{2-\delta}$ electrolyte powder was synthesized by the polyvinyl alcohol assisted combustion method, and then characterized by crystalline structure, powder morphology, sintering micro-structure and electrical properties. The results demonstrate that the as-synthesized $Ce_{0.79}Gd_{0.2}Cu_{0.01}O_{2-\delta}$ was well crystalline with cubic fluorite structure, and exhibited a porous foamy morphology composed of gas cavities and fine crystals ranging from 30 to 50 nm. After sintering at 1100 °C, the as-prepared pellets exhibited a dense and moderate-grained micro-structure with 95.54% relative density, suggesting that the synthesized $Ce_{0.79}Gd_{0.2}Cu_{0.01}O_{2-\delta}$ powder had high sintering activity. The powders made by this method are expected to offer potential application in intermediate-to-low temperature solid-oxide fuel cells, due to its very low densification sintering temperature (1100 °C), as well as high conductivity of 0.026 S cm^{-1} at 600 °C and good mechanical performance with three-point flexural strength value of 148.15 ± 2.42 MPa.

1. Introduction

In recent years, intermediate-to-low temperature solid-oxide fuel cells (SOFCs) with operating temperature range of 500–800 °C have increasingly attracted much attention in scientific community because of their remarkable advantages such as potential long-term stability and economical competitiveness for vehicle and stationary applications [1]. Due to high oxygen-ionic conductivity and good compatibility with electrodes, Gd-doped CeO_2 based ceramics have been popularly known as the most promising electrolytes for solid-oxide fuel cells operating below 600 °C where the electronic contribution in reducing conditions is small. It is well verified that high electrical conductivity can be achieved for 20 mol% Gd-doped ceria, i.e., $Ce_{0.8}Gd_{0.2}O_{2-\delta}$. However, it is still difficult for $Ce_{0.8}Gd_{0.2}O_{2-\delta}$ electrolytes to be densely sintered below 1500 °C for the conventional synthesis method, i.e., the solid state reaction of high-purity CeO_2 and Gd_2O_3 [2]. High sintering temperatures result in a big stumbling block for the fabrication of SOFCs because ceria-based electrolyte and electrodes, cannot be co-fired at temperatures higher than 1300 °C, especially for cathode-supported SOFCs. Also, high temperature sintering leads to partial reduction from Ce^{4+} to Ce^{3+} in the ceria-based materials above 1200 °C.

In order to prepare dense CeO_2 based electrolyte at reduced sintering temperature, three main effective methods have been developed: (1) addition of low melting-point sintering aids using transition metal oxides such as CoO, CuO, MnO_2, Fe_2O_3, Bi_2O_3, Cr_2O_3 and NiO [3–6]. Among them, Cu-, Ni-, and Co-oxides were justified to be very effective in reducing densification sintering temperature, which is as low as 900–1000 °C; (2) specific process treatments such as mechanochemical activation [7] and supercritical drying [8]; (3) adoption of high sintering activity nano-sized powders synthesized by various wet chemical techniques such as sol–gel [9], citrate–nitrate process [10] and co-precipitation [11]. The products derived from these wet-chemical methods usually show better performance due to their high homogeneity in composition. However, the traditional wet-chemical synthesis is complicated and time-consuming, such as in the sol–gel process.

Recently, a lot of interests have been actively focused on the polymer-assisted combustion synthesis, which can produce high-quality nano-sized powders with high specific surface area, homogeneous micro-structure and fewer impurities at very low temperatures [12]. More especially, this technique shows several advantages in the synthesis of multi-component compound powders, which makes dopant incorporate into the lattice by instant combustion and the compound avoid deviating from stoichiometry. As a low-cost and effective fuel, polyvinyl alcohol (PVA) with isolated hydroxyl functional groups not only can adsorb but also complex with metal cations. In aqueous solution, PVA can induce the homogeneous incorporation of metal ions into its polymer network structure and prevent their flocculation or precipitation. As a consequence, PVA has been successfully used in chemical synthesis of high-quality nano-sized powders such as SDC ($Ce_{0.8}Sm_{0.2}O_{1.9}$)

* Corresponding author. Tel.: +353 61202640; fax: +353 61338172.
E-mail addresses: yingchao.dong@ul.ie, dongyc9@mail.ustc.edu.cn (Y. Dong).

0378-7753/$ – see front matter © 2010 Elsevier B.V. All rights reserved.
doi:10.1016/j.jpowsour.2010.03.053

[13], Co_3O_4 [14], cordierite ($2MgO{\cdot}2Al_2O_3{\cdot}5SiO_2$) [15], $CaAl_2O_4$, $Y_4Al_2O_9$, and YPO_4 [16,17], $LiMn_2O_4$ [18], Cr-stabilized ZrO_2 [19] and Nd_2O_3 [20]. However, little research work has reported the synthesis of CGO-based electrolyte powders by this simple PVA assisted combustion process. Rocha and Muccillo firstly prepared nano-crystalline $Ce_{0.8}Gd_{0.2}O_{1.9}$ powder with PVA as fuel and reductant, and mainly studied its powder characteristics from the combustion synthesis process [21].

In our work CuO was selected as sintering promoter with $Cu(NO_3)_3{\cdot}3H_2O$ as precursor because it is proved to be effective in lowering sintering temperature of $Sm_{0.2}Ce_{0.8}O_{1.9}$ electrolyte below 1000 °C when doped at very low level (1 at.%), though a slight decrease in ionic conductivity was observed [22]. Also, 1 mol% CuO was used as sintering aid to lower sintering temperature of gadolinium-doped barium cerate (by ~150 °C), accompanied with higher conductivity in both air and hydrogen atmosphere [23]. Kang and Choi reported that the co-doping of 2 at.% of alumina (as strengthening additive) and 1 at.% Cu (as sintering aid) in 10 mol% Gd-doped ceria show good sintering ability without much loss of electrical conductivity [24]. In this communication, therefore, for the first time to our knowledge, a highly crystalline nano-sized $Ce_{0.79}Gd_{0.2}Cu_{0.01}O_{2-\delta}$ (referred to as CGCO in this paper) electrolyte powder with doped very minor amount of CuO was synthesized by this simple PVA assisted combustion method. The crystalline structure and morphology were respectively characterized by XRD, FE-SEM (Field Emission Scanning Electronic Microscope) and HR-TEM (High Resolution Transmission Electronic Microscope). In addition, the sintering, conductivity, thermal and mechanical properties are preliminarily presented to test the performance of these powders for the possible application as intermediate-to-low temperature SOFC electrolyte. Interestingly, we found that the as-synthesized $Ce_{0.79}Gd_{0.2}Cu_{0.01}O_{2-\delta}$ can be sintered densely at temperature as low as 1100 °C and further that exhibited a remarkably improved electrical conductivity of 0.026 S cm^{-1} at 600 °C.

2. Experimental

2.1. Synthesis and characterization of powders

The PVA combustion synthetic process for nano-sized CGCO powder is very simple. Firstly, the mixed solution with a concentration of 0.5 M cation was obtained by dissolving $Ce(NO_3)_3{\cdot}6H_2O$ (≥99.0%; Sinopharm Chemical Reagent Co., Ltd.), $Cu(NO_3)_3{\cdot}3H_2O$ (≥99.5%; Sinopharm Chemical Reagent Co., Ltd.) and Gd_2O_3 (99.99%) with correct stoichiometric proportion in distilled water and dilute nitric acid, respectively. Subsequently, the 5.00 wt.% aqueous PVA (1750 ± 50; Sinopharm Chemical Reagent Co., Ltd.) solution with specific volume was added to the mixed metal nitrate solution with the molar ratio of PVA monomer to metal cations as 2:1. The excessive water was vaporized during the homogenization of this solution at 90 °C for sufficient time. Then the obtained dried gel was transferred into a 1000 ml ceramic basin above an electrical furnace. The combustion reaction took place dramatically in an instant, accompanied with a slight sound of explosion. Afterwards, the as-synthesized powders were collected for use.

Both dried gel and synthesized powder were directly characterized using XRD (Cu Kα radiation; D8 ADVANCE, Bruker Corporation, Germany). The synthesized CGCO powders before and after ball-milling with zirconia balls in absolute ethyl alcohol for 24 h are observed by FE-SEM (JSM-6700F, JEOL, Japan). HR-TEM (JEM-2010, JEOL, Japan) was also employed to characterize CGCO nano-crystals.

2.2. Dry-pressing, sintering and characterization

The as-synthesized CGCO powders were ball-milled in an ethanol medium for 24 h, and dried subsequently. With PVA-1750 solution (5.00 wt.%) as organic binder, small pellet (Ø15 mm × 0.8 mm) specimens were uniaxially pressed using hydraulic press machine at a pressure of 360 MPa. After drying, the CGCO disc samples were sintered in air at 900–1200 °C for 5 h at an interval of 100 °C. For all the samples, the heating rate was fixed at 1 °C min^{-1} before 550 °C and 2 °C min^{-1} between 550 °C and final temperatures. A holding time of 1 h was carried out at 550 °C in order to remove organic additives added.

The shrinkage percents in diameter direction of the sintered CGCO pellets were measured using a vernier caliper. Both open porosity and relative density were measured in distilled water using the conventional Archimedes' method. Micro-structures of the sintered bodies were observed using FE-SEM as mentioned above.

AC impedance spectroscopy measurements were conducted on electrochemical impedance spectrum analyzer (CHI 600A, Chenhua Inc., Shanghai, PR China) in the frequency range of 0.1–100 kHz. The sintered CGCO pellet (effective diameter: 12.06 mm; thickness: 0.76 mm) was coated with silver paste and fired at 800 °C for 1 h before measurement, and then was put into the tube furnace and heated at a heating rate of 2 °C min^{-1} in air. Measurements were made between 300 and 750 °C in 50 °C steps. In all measurements, the lead resistance was subtracted by measuring the impedance of a blank cell. The conductivity values at different temperatures were calculated according to the following equation:

$$\sigma = \frac{L}{RS} \quad (1)$$

where L is the thickness of the pellets, S the effective area of the measured pellets ($S = 0.25\pi D^2$, D is effective diameter) and R the resistance of the pellets at different temperatures.

Thermal expansion co-efficient of the sintered CGCO was measured between room temperature (26 °C) and 1000 °C in a horizontal dilatometer (DIL 402C, Netzsch, Germany). A constant heating rate of 10 °C min^{-1} was used. The length change was recorded with a dense α-alumina as reference sample. Room temperature flexural strength was determined by the three-point bending method in a universal materials testing machine (3369, Instron Corporation, USA). A span length of 30 mm and crosshead speed of 0.5 mm min^{-1} were used. All the tested bars were polished and beveled in advance by 360-mesh and then 800-mesh metallographic sandpapers in order to eliminate surface stress.

3. Results and discussion

3.1. XRD pattern

Fig. 1 shows the XRD patterns of the CGCO dried gel and as-synthesized powder. It can be seen that the CGCO-based polymer gel is amorphous to X-rays, suggesting that all the metal cations (Ce^{3+}, Gd^{3+} and Cu^{2+}) are physically entrapped and then chemically bound with hydroxyl functional groups of large chain molecule PVA. This therefore resulted in a homogeneous distribution of metal cations at an atom scale in the network of the dried polymer carrier during the process. In this PVA solution process, a homogeneously mixed solution was easily obtained by completely dissolving as-required metal nitrates without any adjustment of solution pH, especially compared with the mixed sol–gel processing route. After combustion, the CGCO had an appearance of a light brown powder, which is different with the typical one of $Ce_{0.8}Gd_{0.2}O_{1.9}$ (light yellow), maybe because of the effluence of minor amount of Cu(II) element added, which existed as in the form of CuO with transition color from blue to black brown.

The as-synthesized CGCO powder is well crystalline in nature with phase-pure CeO_2 of cubic fluorite structure. The diffraction

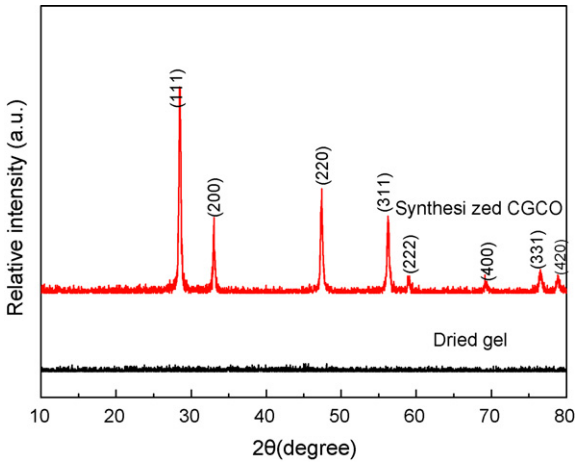

Fig. 1. XRD patterns of the CGCO dried gel and as-synthesized powder.

peaks could be indexed according to a cubic fluorite lattice (*Fm*3*m* space group). The redox combustion reaction between PVA and metal nitrates was initiated at very low temperature at about 250–300 °C, indicated by a slight sound of explosion in the experiments, which is slightly different with the initiation temperature of 220 °C [17] because of the difference of starting material ratio. As a consequence, a large quantity of reaction heat was released. This resulted in relatively high temperature for the reaction system in a short time, which was favor to cause the sufficient crystallization of nano-sized CGCO materials. The lattice parameter and lattice volume were calculated from the obtained XRD pattern, those of the un-doped sample (CGO) is also displayed for comparison, as shown in Table 1. The lattice parameter of the as-synthesized CGCO powder is 5.4086 nm, which a little lower than that of the CGO (a = 5.4195 nm). Such a decrease in both lattice parameter and lattice volume after Cu doping is due to the substitution of smaller Cu^{2+} ions (r = 0.073 nm) for Ce^{4+} ions (r = 0.097 nm) in the cubic lattice of the $Ce_{0.8}Gd_{0.2}O_{2-\delta}$ structure [25].

3.2. SEM and TEM

Fig. 2 presents the SEM and enlarged TEM micro-photographs of the CGCO powder. The CGCO agglomerates exhibit a highly porous foam micro-structure, which consists of gas cavities and fine CGCO crystals (Fig. 2a). This porosity resulted from the gases instantly released by the intense redox reaction of PVA and metal nitrates at fuel-rich conditions. PVA networks not only acted as fuel and reductant, but also maintained the pore structures of the gel precursors, thus preventing particle agglomeration to some extent. This also indicates that the chemical combustion reaction occurred in the CGCO was quite intense. This highly porous structure is quite typical for the nano-sized powders prepared by the polymer-assisted combustion technique [13–20]. Also we found that in the experiments the as-synthesized CGCO powder was quite friable due to its sponge-like structure. The large agglomerates were easily broken up into micro-sized particles after ball-milling, which are still agglomerated (Fig. 2b).

Table 1
Lattice parameter and lattice volume of the un-doped (CGO) and doped (CGCO) samples after combustion reaction.

	CGO	CGCO
Lattice volume	159.1729	158.2147
Lattice parameter	5.4195	5.4086

Table 2
Radial shrinkage percent, open porosity and relative density of the CGCO compacts sintered at different temperatures for 5 h.

Sintering temperature (°C)	900	1000	1100	1200
Shrinkage percent (%)	15.24	18.33	18.92	19.62
Open porosity (%)	13.46	0	0	0
Relative density (%)	83.92	96.33	95.54	94.48

From the TEM micro-photograph (Fig. 2c), it can be still confirmed that this porous agglomerated micro-structure with high magnification appears for the ball-milled CGCO particles. From Fig. 2d, it clearly shows the formation of nano-sized CGCO crystals with uniform size and compact distribution. Most of crystalline grains in the CGCO powder have a crystalline size range of 30–40 nm, with the exception of a small quantity of grains larger than 50 nm. The observed crystalline grains for the CGCO are of roughly hexagonal shape with corners and edges, and compact with each other. This compact state of CGCO grains in the as-synthesized powder might be due to strong agglomeration during high temperature combustion, resulting from the released heat via the reaction of PVA and metal nitrates. The selected area electron diffraction pattern (SAED), shown in Fig. 2e, exhibits eight broad rings which could be attributed to (1 1 1), (2 0 0), (2 2 0), (3 1 1), (2 2 2), (4 0 0), (3 3 1) and (4 2 0) reflections of the cubic fluorite structure of CeO_2, respectively.

3.3. Sintering and micro-structure

The as-synthesized CGCO had high sintering activity, which is justified by the following measurements, including shrinkage percent, relative density and SEM of the sintered bodies.

Table 2 presents radial shrinkage percent, open porosity and relative density of the dry-pressed CGCO compacts sintered at 900–1200 °C for 5 h. An obvious increase in both shrinkage percent and relative density exists from 900 to 1000 °C, indicating that a quick densification process occurred in this temperature range. The open porosity is 13.46% at 900 °C, but decreases up to 0 for all the samples sintered above 1000 °C. This quick densification at low sintering temperature could be ascribed to the formation of a new Gd_2O_3–CeO_2–CuO ternary liquid phase in the grain boundaries of the sample with minor amount of Cu element, which resulted in quick densification due to the liquid phase diffusion under capillary action along with grain rearrangement during sintering [26]. In the presence of a small amount of liquid, the densification process could be considered as taking place due to the elimination of solid–vapor interface by the liquid, where the densification driving force is the decrease of liquid–vapor interface area. This is different from the un-doped Gd_2O_3–CeO_2 solution ($Ce_{0.8}Gd_{0.2}O_{2-\delta}$), in which the sintering is mainly dominated by a solid-state diffusion mechanism [27], where high temperature is necessary to complete sintering densification process. Such a suggestion is in close agreement with that reported on the low-temperature sintering behavior for $Ce_{0.9}Gd_{0.1}O_{1.95}$ doped with copper element at levels of 1–3 mol% by Nicholas and De Jonghe [28], attributed to the formation of liquids in the high temperature reaction of Gd_2O_3, CeO_2 and CuO. A similar reduction behavior in sintering temperature for $Ce_{0.8}Gd_{0.2}O_{2-\delta}$ has been also obtained with the addition of minor amount of Co element [29]. For the sample sintered at 1000 °C, the relative density is as high as 96.33%, and its radial shrinkage percent is 18.33%. But with increasing temperature further from 1000 to 1100 °C, the CGCO shows further sintering shrinkage from 18.33% to 18.92%, as well as a slight decrease from 96.33% to 95.54% in relative density. A similar change trend exists for the samples sintered between 1100 and 1200 °C. The slight decrease of relative density with sintering temperature (between

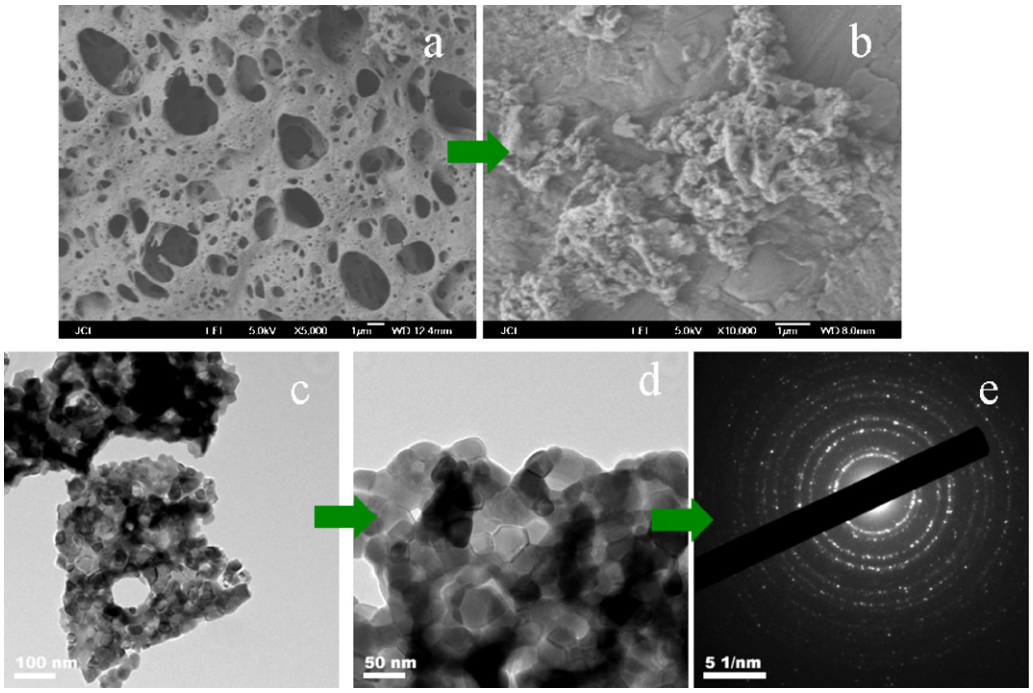

Fig. 2. Micro-photographs of the as-prepared CGCO powders: (a) SEM picture for as-synthesized CGCO; (b) SEM picture for ball-milled CGCO; (c) low magnification TEM picture for ball-milled CGCO; (c) high magnification TEM picture for ball-milled CGCO; (e) SAED pattern of CGCO poly-crystals.

1000 and 1200 °C) may be attributed to the retard of inter-granular pore elimination process during viscous flow sintering induced by the formed multiple oxides liquid phase at higher temperatures.

Fig. 3 illustrates the surface and cross-section SEM micro-structures of the CGCO sample sintered at 1100 °C for 5 h, with high relative density (95.54%). A typical dense micro-structure is observed (Fig. 3a), which indicates a moderate grain growth. The grain size in the CGCO sintered body varies in the range of 1.0–3.0 μm. During low-temperature sintering, the formed Gd_2O_3–CeO_2–CuO ternary liquid phase in grain-boundary accelerated mass transport due to its dissolution and precipitation from the melt, therefore resulting in quick sintering densification at relatively low temperatures. There are small amount of closed gas pores existing in the sintered sample, as observed from the cross-section micro-graph (Fig. 3b).

3.4. Electrical conductivity, thermal and mechanical properties

Fig. 4 shows the Arrhenius plot of $\ln(\sigma T)$ versus $1000/T$ for the CGCO sample sintered at 1100 °C for 5 h. The activation energy can

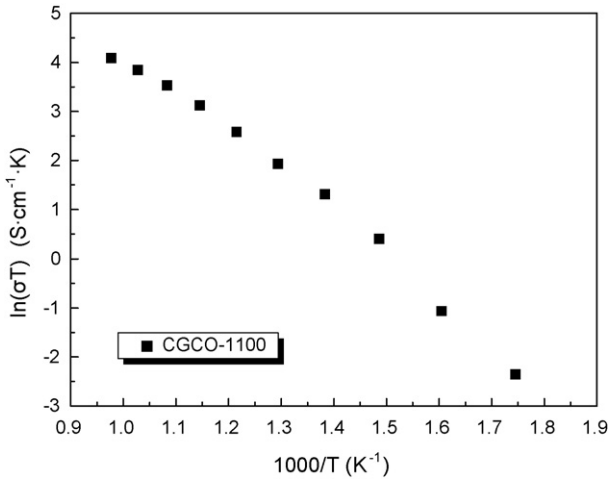

Fig. 4. Relationship between conductivity and temperature.

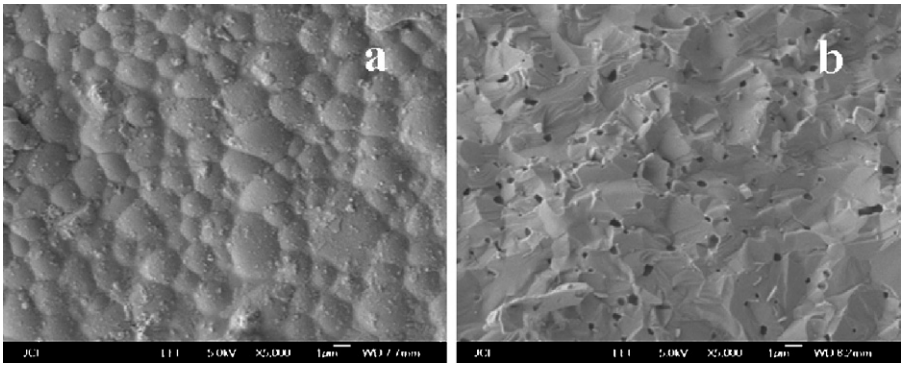

Fig. 3. SEM micro-graphs of the CGCO sample sintered at 1100 °C for 5 h: (a) surface and (b) fractural surface.

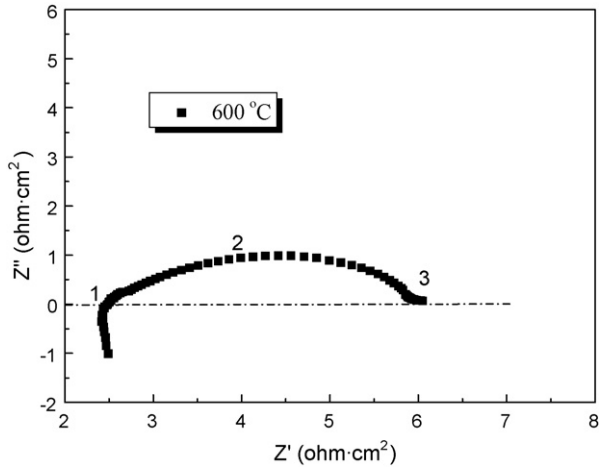

Fig. 5. AC impedance spectrum of the sintered CGCO ceramic measured at 600 °C.

be calculated from the following Arrhenius equation:

$$\sigma = \left(\frac{\sigma_0}{T}\right) \exp\left(\frac{-Ea}{kT}\right) \quad (2)$$

where σ, σ_0, Ea, k and T are conductivity, pre-exponential factor, activation energy, Boltzmann constant ($K = 1.3806505 \times 10^{-23}\,\mathrm{J\,K^{-1}}$) and absolute temperature, respectively. The activation energy of CGCO was 1.164 eV, which was calculated from the slope of the plot in Fig. 4.

The conductivity is 0.026 S cm^{-1} at a measurement temperature of 600 °C, which is much higher than the as-reported CGO ceramics (0.016 S cm^{-1} at 600 °C), mainly due to increase of oxygen-ionic conductivity [30]. Also, interestingly, this electrical conductivity value is slightly higher than that (0.021 S cm^{-1}) in the cobalt-doped 20 mol% Gd-doped CeO_2 ($Ce_{0.79}Gd_{0.2}Co_{0.01}O_{2-\delta}$) [29], regardless of slightly lower relative density of $Ce_{0.79}Gd_{0.2}Cu_{0.01}O_{2-\delta}$ (95.54%) in our work. The high electrical conductivity could be ascribed to the coarse grains in the dense CGCO sintered body, in which grain boundary electrical resistance is small [31]. Fig. 5 shows the impedance spectra measured at 600 °C for the CGCO sample sintered 1100 °C. Arcs 1, 2 and 3 respond to the grain interior, grain boundary, and the polarization of electrodes, respectively. The spectrum is similar with the general form for different samples. It is suggested that the addition of minor amount of Cu is a quite effective method to prepare doped CGO powder with excellent electrical performance.

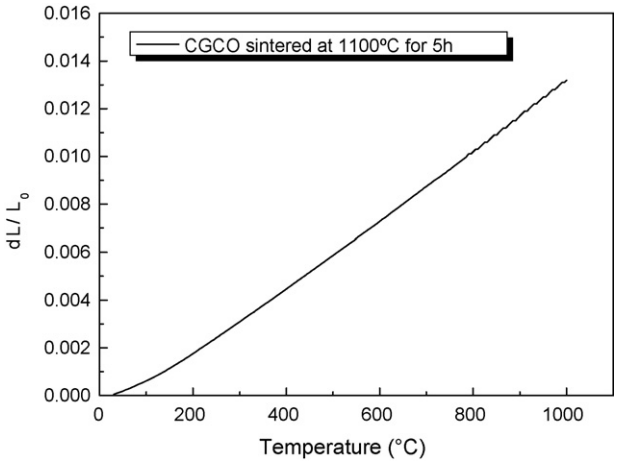

Fig. 6. Thermal expansion curve of the CGCO ceramic sintered at 1100 °C for 5 h.

Fig. 6 presents the thermal expansion curve of the CGCO ceramic after sintering at 1100 °C for 5 h. The sample exhibits a general expansion behavior during heating. Between room temperature (26 °C) and 1000 °C, the average thermal expansion co-efficient is $13.55 \times 10^{-6}\,\mathrm{K^{-1}}$, which is higher than that of the commonly used SOFC electrolyte YSZ ($\sim 10.8 \times 10^{-6}\,\mathrm{K^{-1}}$). In the low temperature range of 26–600 °C, the average thermal expansion co-efficient is $12.67 \times 10^{-6}\,\mathrm{K^{-1}}$.

Furthermore, the CGCO electrolyte sintered at 1100 °C for 5 h exhibited a good mechanical performance and its three-point flexural strength is 148.15 ± 2.42 MPa when tested at room temperature (23 °C).

4. Conclusions

In this communication, we reported an easily synthesized $Ce_{0.79}Gd_{0.2}Cu_{0.01}O_{2-\delta}$ electrolyte with densification sintering temperature as low as 1100 °C, as well as high electrical conductivity. After combustion reaction with polyvinyl alcohol as effective fuel and reductant, the $Ce_{0.79}Gd_{0.2}Cu_{0.01}O_{2-\delta}$ powder showed a well crystalline structure of cubic fluorite, and a porous foamy morphology composed of gas cavities and fine crystals ranging from 30 to 50 nm. After sintering at 1100 °C for 5 h, the as-prepared $Ce_{0.79}Gd_{0.2}Cu_{0.01}O_{2-\delta}$ pellets exhibited a dense micro-structure with 95.54% of theoretical density, conductivity of 0.026 S cm^{-1} (at 600 °C), and good room temperature three-point flexural strength of 148.15 ± 2.42 MPa. Furthermore, the densification sintering temperature of the CGCO is very close to the processing temperature of cathode components, which offers the possibility of co-sintering with cathode components during fabrication of cathode-supported SOFCs.

Acknowledgements

Prof. S. Hampshire and Dr. Y. Dong wish to thank the Irish Research Council for Science, Engineering and Technology (IRCSET) for financial support (IRCSET EMPOWER post-doctoral grant). The authors also would like to acknowledge technical staffs (Mr. Nigel Coleman, Mr. Clive Considine, Ms. Catherine Johnson) and Dr. Abde, Dr. Clare and Dr. Declan for their assistance in research.

References

[1] B. Steele, A. Heinzel, Nature 414 (2001) 345.
[2] M. Chourashiya, J. Patil, S. Pawar, L. Jadhav, Mater. Chem. Phys. 109 (2008) 39.
[3] V. Gil, J. Tartaj, C. Moure, P. Duran, J. Eur. Ceram. Soc. 26 (2006) 3161.
[4] C. Kleinlogel, L. Gauckler, Solid State Ionics 135 (2000) 567.
[5] C. Kleinlogel, L.J. Gauckler, Adv. Mater. 13 (2001) 1081.
[6] W. Zając, L. Suescun, K. Świerczek, J. Molenda, J. Power Sources 194 (2009) 2.
[7] W.S. Jung, H.S. Park, Y.J. Kang, D.H. Yoon, Ceram. Int. 36 (2010) 371.
[8] J.P. Liang, Q.S. Zhu, Z.H. Xie, W.L. Huang, C.Q. Hu, J. Power Sources 194 (2009) 640.
[9] T. Yu, J. Joo, Y. Park, T. Hyeon, Angew. Chem. 117 (2005) 7577.
[10] R. Rocha, E. Muccillo, Cerâmica 47 (2001) 219.
[11] T. Zhang, L. Kong, P. Hing, Y. Leng, S. Chan, J. Kilner, J. Power Sources 124 (2003) 26.
[12] S. Aruna, A. Mukasyan, Curr. Opin. Solid State Mater. Sci. 12 (2008) 44.
[13] J. Ma, C. Jiang, X. Zhou, G. Meng, X. Liu, J. Power Sources 162 (2006) 1082.
[14] J. Jiu, Y. Ge, X. Li, L. Nie, Mater. Lett. 54 (2002) 260.
[15] S. Lee, W. Kriven, J. Am. Ceram. Soc. 81 (1998) 2605.
[16] S. Lee, P. Shin, J. Kim, S. Chun, Mater. Sci. Forum 21 (2007) 534.
[17] M. Gulgun, M. Nguyen, W. Kriven, J. Am. Ceram. Soc. 82 (1999) 556.
[18] A. Subramania, N. Angayarkanni, T. Vasudevan, Mater. Chem. Phys. 102 (2007) 19.
[19] J. Ray, C. Saha, P. Pramanik, J. Eur. Ceram. Soc. 22 (2002) 851.
[20] W. Yang, Y. Qi, Y. Ma, X. Li, X. Guo, J. Gao, M. Chen, Mater. Chem. Phys. 84 (2004) 52.
[21] R. Rocha, E. Muccillo, Br. Ceram. Trans. 102 (2003) 216.
[22] X.G. Zhang, C. Deces-Petit, S. Yick, M. Robertson, O. Kesler, R. Maric, D. Ghosh, J. Power Sources 162 (2006) 480.
[23] E. Gorbova, V. Maragou, D. Medvedev, A. Demin, P. Tsiakaras, J. Power Sources 181 (2008) 292.

[24] Y.J. Kang, G.M. Choi, Solid State Ionics 180 (2009) 886.
[25] R. Shannon, Acta Crystallogr. A32 (1976) 75.
[26] J. Mackenzie, R. Shuttleworth, Proc. Phys. Soc. Lond. 62 (1949) 633.
[27] T. Zhang, P. Hing, H. Huang, J. Kilner, J. Eur. Ceram. Soc. 21 (2001) 2222.
[28] J. Nicholas, L. De Jonghe, Solid State Ionics 178 (2007) 1187.
[29] A. Dutta, A. Kumar, R.N. Basu, Electrochem. Commun. 11 (2009) 699.
[30] D. Fagg, J. Abrantes, D. Perez-Coll, P. Nunez, V. Kharton, J. Frade, Electrochim. Acta 48 (2003) 1023.
[31] R. Gerhardt, Nowick, J. Am. Ceram. Soc. 69 (1986) 641.